Progress In Electromagnetics Research, PIER 83, 225–244, 2008

RECTANGULAR WAVEGUIDE-FED HEMISPHERICAL DIELECTRIC RESONATOR ANTENNA

P. Abdulla and A. Chakrabarty

Department of Electronics and Electrical Communication Engineering
Indian Institute of Technology
Kharagpur 721302, West Bengal, India

Abstract—Hemispherical dielectric resonator (HDR) antenna excited with a thick slot at the short circuited end of waveguide is analyzed theoretically and verified experimentally. The problems are formulated using the Green's function approach; with unknown slot currents solved using the method of moments (MOM). The HDR is modeled using exact magnetic field Green's function due to the equivalent magnetic current in the slot. The field inside the waveguide is expressed in terms of model vectors and modal functions. Thickness of the slot is analyzed using cavity approach. For the analysis of HDR antenna part, the modal series is represented as a sum of particular and homogeneous solutions. The particular solution is computed efficiently using spectral domain approach. In order to determine the effects of varying design parameters on bandwidth and matching, sensitivity analysis is carried out using the code developed. Measurements were carried out to verify the theory, and reasonable agreement between them is obtained.

1. INTRODUCTION

It has been shown that dielectric resonator antennas (DRA) can be used as effective radiators at microwave frequencies where ohmic losses become a serious problem for conventional metallic antennas [1–4]. DRAs offer several advantages such as small size, low cost, light weight, ease of excitation and ease of integration with active circuitry. They offer wider bandwidth than the microstrip antennas used at the same frequency [5–8].

Many different feeding mechanisms can be used with DRA, such as the co-axial probe [9], direct microstrip line feed [10, 11], aperture coupled by microstripline or coplanar waveguide [12–14] and conformal strip feed [15]. However, feed line losses of these excitation methods are

considerable at millimeter-wave frequencies. Today, the waveguide still plays an important role in microwave and millimeter-wave applications; it is the basic unit of many microwave/millimeter-wave components such as magic Tees, directional couplers, phase shifters and filters. Since the waveguide has metallic walls, it has an excellent shielding between the exterior and interior regions, thus avoiding radiation loss even in the millimeter–wave band. Recently, a new and low loss excitation scheme that employs a rectangular waveguide broad wall slot fed is reported [16], in which analysis is given for the broad wall slot coupled cylindrical dielectric resonator only. Moreover, the DR is analyzed using the body of revolution, which is applicable only for symmetrical structures. The analysis of aperture coupled hemispherical dielectric resonator antenna (HDRA) with microstrip as feed line has been done in [17] using modal series method, in which, the modal series is represented as a sum of particular and homogeneous solutions. The particular solution given is a slowly convergent series and it takes a lot of computation time. This is because the value of Hankel function becomes very large while their argument reduces. It takes days together to get the result. The alternative method of magnetic dipole suggested by the author is valid only for narrow slots. In this paper, the particular solution, which represents the source radiating in the unbounded dielectric medium, is obtained using spectral domain approach [18, 19]. The thick slot on the ground plane is analyzed as a rectangular cavity. The analysis of this rectangular cavity is done using Green's function approach. Since the fundamental mode, TE_{111} of the DRA used is 7.15 GHz, it is excited at TE_{211} mode to resonate the DRA in the X-band [9, 12]. The fields inside the waveguide are considered using modal vectors and modal functions. The power coupling to DRA is computed and measured. The computed and measured results are again compared with commercial FEM code (Ansoft HFSS) simulating software [22]. To check the sensitivity analysis, parametric study is carried out using the code developed.

2. FORMULATION

The geometry of the waveguide shorted end slot coupled HDRA is shown in Fig. 1. The cross sectional and front view of Fig. 1, for the detailed analysis is shown in Fig. 2. We assume that the ground plane of thickness $2t$ on which HDRA sitting is extend to infinity in the $\hat{x}$ and $\hat{y}$ directions. The considered slot is narrow in $\hat{y}$ direction to eliminate any possible cross-polarization, only variation along x is considered for magnetic field, i.e., the electric field E_y in the aperture varies only in the x-direction and is non-varying in the y direction.

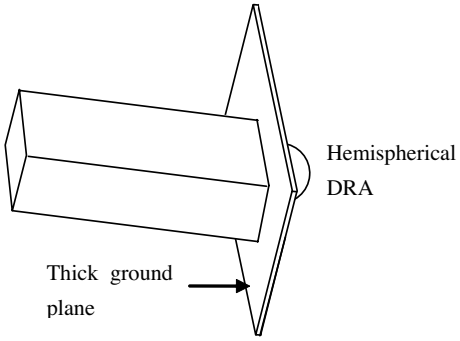

Figure 1. Configuration of the waveguide fed hemispherical DRA.

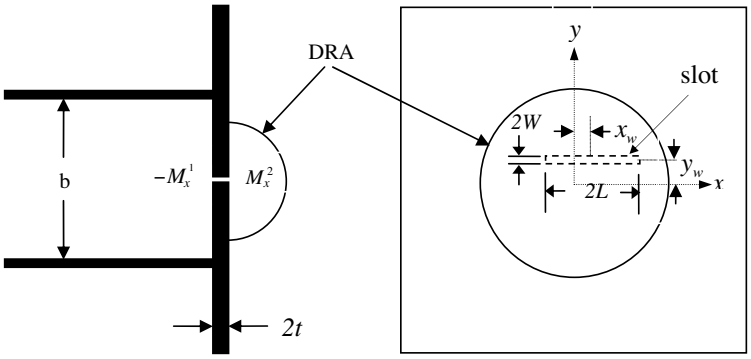

Figure 2. Longitudinal cross section and front view of the proposed structure.

At the region of the slot, the tangential component of the magnetic fields both inside the waveguide and outside (within the DR) should be identical. Invoking the surface equivalence principle, the slot can be closed by a perfect electric conductor which divides the problem into two equivalent problems: the slotted waveguide part and the DRA placed on the infinite ground plane. By applying magnetic boundary conditions at the apertures of waveguide and slot, and slot and DRA, the magnetic field $H(\bar{M})$ can be expressed as:

$$2H_x^{inc} - H_x^{WG}(\bar{M}_x^1) - H_x^{SL}(\bar{M}_x^1) + H_x^{SL}(\bar{M}_x^2) = 0 \quad (1)$$

$$H_x^{SL}(\bar{M}_x^1) - H_x^{SL}(\bar{M}_x^2) - H_x^{DRA}(\bar{M}_x^2) = 0 \quad (2)$$

where $H_x^{\alpha}\left(\bar{M}_x^i\right)(i = 1,\ 2$ and $\alpha = WG, SL, DRA)$ is the magnetic fields due the magnetic currents at the aperture i, any of the two faces

of the thick slot, 1 and 2. If E^i_{yp} is the unknown coefficient for the electric field at the aperture, then the electric field is assumed to be of the form.

$$\bar{E}^i_y\left(x'\right) = \hat{u}_y \sum_{p=1}^{M} E^i_{yp} e^i_p\left(x'\right) \tag{3}$$

where, $e^i_p\left(x'\right)$ $(p = 1, 2, 3, \ldots, M)$ are defined by

$$e^i_p\left(x'\right) = \begin{cases} \sin\left[\dfrac{p\pi}{2L_i}\left(x' - x_{wi} + L_i\right)\right], & \begin{array}{c} x_{wi} - L_i \le x' \le x_{wi} + L_i \\ y_{wi} - W_i \le y' \le y_{wi} + W_i \end{array} \\ 0, & \text{elsewhere} \end{cases} \tag{4}$$

For Galerkin's procedure of method of moments, the weighing function is same as testing and is given by

$$e^i_q\left(x\right) = \begin{cases} \sin\left[\dfrac{q\pi}{2L_i}\left(x - x_{wi} + L_i\right)\right], & \begin{array}{c} x_{wi} - L_i \le x \le x_{wi} + L_i \\ y_{wi} - W_i \le y \le y_{wi} + W_i \end{array} \\ 0, & \text{elsewhere} \end{cases} \tag{5}$$

H^{inc}_x is the x component of incident magnetic field at the aperture 1 for transmitting mode is the dominant TE_{10} mode, and is given by [23]

$$H^{inc}_x = -Y_0 \cos\left(\frac{\pi x}{2a}\right) e^{-j\beta z} \tag{6}$$

The magnetic field scattered inside the slot region ($H^{SL}_x(\bar{M}^1_x)$, $H^{SL}_x(\bar{M}^2_x)$) are determined by using cavity Green's function of the electric vector potential. The cavity Green's function has been derived by solving the Helmholtz equation for the electric vector potential for the unit magnetic current source. The x-component of the Green's function is

$$\begin{aligned} G_{xx} = & \sum_{m=1}^{\infty}\sum_{n=0}^{\infty} \frac{\varepsilon_m \varepsilon_n}{4LW} \sin\left[\frac{m\pi}{2L}\left(x+L\right)\right] \sin\left[\frac{m\pi}{2L}\left(x'+L\right)\right] \cos\left[\frac{n\pi}{2W}\left(y+W\right)\right] \\ & \times \cos\left[\frac{n\pi}{2W}\left(y'+W\right)\right] \frac{-1}{\Gamma_{mn}\sin\left(2\Gamma_{mn}t\right)} \\ & \begin{cases} \cos\left[\Gamma_{mn}\left(z-t\right)\right]\cos\left[\Gamma_{mn}\left(z'+t\right)\right] & z > z' \\ \cos\left[\Gamma_{mn}\left(z'-t\right)\right]\cos\left[\Gamma_{mn}\left(z+t\right)\right] & z < z' \end{cases} \end{aligned} \tag{7}$$

where

$$\Gamma_{mn} = \sqrt{k^2 - \left(\frac{m\pi}{2l}\right)^2 - \left(\frac{n\pi}{2w}\right)^2} \quad \text{and} \quad \varepsilon_i = \begin{cases} 1, & i = 0 \\ 2, & i \neq 0 \end{cases} \tag{8}$$

The electric vector potential $\bar{F}$ in terms of Green's function is given by

$$\bar{F}(r) = \int_{r'} G_{xx}\left(r/r'\right)\bar{M}\left(r'\right)dr' \tag{9}$$

The scattered magnetic field inside the cavity region (inside slot) due to the magnetic currents can be determined from

$$\bar{H} = -j\omega\varepsilon\left[\tilde{I} + \frac{\bar{\nabla}\bar{\nabla}}{k^2}\right]\bar{F} \tag{10}$$

X-component of the scattered magnetic fields inside the waveguide region, due to the presence of the magnetic current at the slot aperture is solved from Equation (10) by modal expansion approach [12] and is given by

$$\begin{aligned} &H_x^{WG}\left(M_x^1\right) = \\ &-2LW\sum_m\sum_n\left[Y_{mn}^e\left(C_{mn}^e\frac{m\pi}{2a}\right)^2 + Y_{mn}^m\left(C_{mn}^m\frac{n\pi}{2b}\right)^2\right]\sin\left[\frac{m\pi}{2a}(x+a)\right] \\ &\times\cos\left[\frac{n\pi}{2b}(y+b)\right]\cos\left[\frac{n\pi}{2b}(y_w+b)\right]\operatorname{sinc}\left(\frac{n\pi}{2b}W\right)F_x(p) \end{aligned} \tag{11}$$

where $F_x(p)$ is

$$\begin{aligned} F_x(p) \;=\; &\left\{\cos\left[\frac{\pi}{2}\left(-\frac{mx_w}{a_i}+p-m\right)\right]\operatorname{sinc}\left[\frac{\pi L}{2}\left(\frac{p}{L}-\frac{m}{a_i}\right)\right]\right. \\ &\left.-\cos\left[\frac{\pi}{2}\left(\frac{mx_w}{a_i}+p+m\right)\right]\operatorname{sinc}\left[\frac{\pi L}{2}\left(\frac{p}{L}+\frac{m}{a_i}\right)\right]\right\} \end{aligned} \tag{12}$$

$$C_{mn}^e = \frac{1}{\pi}\sqrt{\frac{ab\varepsilon_m\varepsilon_n}{(mb_i)^2+(na_i)^2}};\quad C_{mn}^m = \frac{2}{\pi}\sqrt{\frac{ab}{(mb)^2+(na)^2}} \tag{13}$$

$$Y_{mn}^e = \frac{k_z}{\omega\mu} = \frac{k_z}{k\eta};\quad Y_{mn}^m = \frac{\omega\varepsilon}{k_z} = \frac{k}{k_z\eta} \tag{14}$$

x_w and y_w are the slot off sets along x and y directions respectively.

Similarly X-component of scattered magnetic field inside the slot

region is

$$H_x^{SL}\left(M_x^i\right) =$$
$$-\frac{j\omega\varepsilon}{k^2}\sum_{p=1}^{M}E_{yp}^{i}\sum_{m=1}^{\infty}\sum_{n=0}^{\infty}\frac{\varepsilon_m\varepsilon_n L_i W_i}{2a_2b_2}\left\{k^2-\left(\frac{m\pi}{2a_2}\right)^2\right\}\sin\left\{\frac{m\pi}{2a_2}\left(x+a_2\right)\right\}$$
$$\times\cos\left\{\frac{n\pi}{2b_2}\left(y+b_2\right)\right\}\cos\left\{\frac{n\pi}{2b_2}\left(y_w+b_2\right)\right\}\operatorname{sinc}\left\{\frac{n\pi}{2b_2}W_i\right\}F_x\left(p\right)$$
$$\times\frac{(-1)}{\Gamma_{mn}\sin\left\{2\Gamma_{mn}t\right\}}\begin{cases}\cos\left\{\Gamma_{mn}\left(z-t\right)\right\}\cos\left\{\Gamma_{mn}\left(z_0+t\right)\right\} & z>z_0\\ \cos\left\{\Gamma_{mn}\left(z_0-t\right)\right\}\cos\left\{\Gamma_{mn}\left(z+t\right)\right\} & z<z_0\end{cases} \quad (15)$$

In the present problem the slot is assumed narrow, only the x-component of the magnetic field at the slot is considered. i.e., the x-component of electric field at the apertures are ignored. The electric field E_y in the aperture varies only in the x-direction and is non-varying in the y direction.

2.1. Green's Function of HDRA and Evaluation of H_x^{DRA}

H_x^{DRA} is the tangential component of the magnetic field coupled to the DRA. For the determination of magnetic field inside the DRA due to the x directed magnetic current, M_x^2, x component of the Green's function, $G_{M_x}^{H_x}$ is required. In the following formulation, the fields are assumed to vary harmonically as $e^{j\omega t}$ which is suppressed. Further more $\mathbf{r}(r,\theta,\phi)$ refers to the field point while $\mathbf{r}(r',\theta',\phi')$ refers to the source point. To begin with, the image theory is employed for determining the Green's function of the DRA. The procedure for deriving the various potential functions is similar to that in coaxial probe fed hemispherical DRA [9] and is therefore not repeated here. The $\hat{x}$-directed magnetic current M_x on the plane $z=0$ is then decomposed in to an $\hat{r}$ directed component M_r and a $\hat{\boldsymbol{\varphi}}$ directed component M_ϕ. The Green's function $G_{M_r}^{F_r}$ denotes the electric potential due to an $\hat{r}$ directed magnetic point current, while the Green's function $G_{M_\phi}^{F_r}$ and $G_{M_\phi}^{A_r}$ denote, respectively, the electric potential and the magnetic potential due to a $\hat{\boldsymbol{\varphi}}$ directed one. To derive the DR Green's function $G_{M_x}^{H_x}$ we define two dyadic Green's function

$$\overline{\overline{G_{M_r}^{H}}} = G_{M_r}^{H_r}\hat{\mathbf{r}}\hat{\mathbf{r}}+G_{M_r}^{H_\theta}\hat{\boldsymbol{\theta}}\hat{\mathbf{r}}+G_{M_r}^{H_\phi}\hat{\boldsymbol{\varphi}}\hat{\mathbf{r}} \quad (16)$$
$$\overline{\overline{G_{M_\phi}^{H}}} = G_{M_\phi}^{H_r}\hat{\mathbf{r}}\hat{\mathbf{r}}+G_{M_\phi}^{H_\theta}\hat{\boldsymbol{\theta}}\hat{\mathbf{r}}+G_{M_\phi}^{H_\phi}\hat{\boldsymbol{\varphi}}\hat{\mathbf{r}} \quad (17)$$

where $G_{M_\alpha}^{H_\beta}(\alpha = r, \phi$ and $\beta = r, \theta, \phi)$ is the magnetic field Green's function derived from G_{Mr}^{Fr}, $G_{M\varphi}^{Fr}$ and $G_{M\varphi}^{Ar}$ using Equations (6)–(26) of Harrington [23]. The total magnetic field excited by M_x is then given by

$$\mathbf{H} = \iint\limits_{So} \left[\overline{\overline{G_{M_r}^H}}.\left(M_r'\hat{\mathbf{r}}\right) + \overline{\overline{G_{M_\phi}^H}}.\left(M_\phi'\hat{\boldsymbol{\varphi}}\right)\right] ds' \tag{18}$$

Now extract the $\hat{\mathbf{x}}$-directed magnetic field H_x from (18) and compare it with the following

$$H_x(x,y) = \iint\limits_{So} G_{M_x}^{H_x}(x,y;x',y')M_x(x',y')ds' \tag{19}$$

the desired Green's function $G_{M_x}^{H_x}$ is derived. Assuming G_{PS} and G_{HS} as the particular and homogeneous solutions respectively, of $G_{M_x}^{H_x}$, then,

$$G_{M_x}^{H_x} = G_{PS} + G_{HS} \tag{20}$$

The field radiated by particular solution and homogeneous solution are evaluated separately to enhance the computation. In this paper, the particular solution, which represents the source radiating in the unbounded dielectric medium, is obtained using spectral domain approach [18]. The X-component of field radiated into unbounded dielectric medium, due to the particular solution, G_{PS} is derived in [10] and therefore not explained here.

$$\begin{aligned} G_{spec} = H_x^{unbouded} = & -\frac{WL}{\pi^2 k\eta}\sum_{p=1}^{M} E_p \int\limits_{-\infty}^{\infty}\int\limits_{-\infty}^{\infty} \frac{k^2-k_z^2}{\left(k^2-k_x^2-k_y^2\right)^{1/2}}\mathrm{sinc}\left(k_x W\right) \\ & \frac{\left\{\begin{array}{ll} j\sin\left(k_z L\right) & \text{for p even} \\ \cos\left(k_z L\right) & \text{for p odd}\end{array}\right\}}{\dfrac{\mathrm{p}\pi}{2}\left\{1-\left(\dfrac{2Lk_z}{p\pi}\right)^2\right\}} e^{j\{k_x x + k_z z\}} dk_x dk_z \end{aligned} \tag{21}$$

$$\begin{aligned} G_{HS} = & -\frac{\cos\phi}{4\pi\omega\mu_0 k}.\frac{\cos\phi'}{r^2 r'^2}\sum_{n=1}^{\infty} g_n n(n+1)(2n+1) \\ & \times P_n(\cos(\phi-\phi'))\hat{J}_n(kr')\hat{J}_n(kr) \\ & + \frac{\cos\phi}{4\pi\omega\mu_0}.\frac{\sin\phi'}{r^2 r'}\sum_{n=1}^{\infty} g_n n(2n+1)\frac{\partial}{\partial\phi}(2n+1) \\ & \times P_n(\cos(\phi-\phi'))\hat{J}_n(kr')\hat{J}_n(kr) \end{aligned}$$

$$
\begin{aligned}
&+\frac{\sin\phi}{4\pi\omega\mu_0}.\frac{\cos\phi'}{rr'^2}\sum_{n=1}^{\infty}g_n n(2n+1)\frac{\partial}{\partial\phi}\\
&\times P_n(\cos(\phi-\phi'))\hat{J}_n(kr')\hat{J}'_n(kr)\\
&-\frac{\omega\varepsilon}{4\pi k}.\frac{\sin\phi\sin\phi'}{rr'}\sum_{n=1}^{\infty}h_n\frac{2n+1}{n(n+1)}\\
&\times P'_n(\cos(\phi-\phi'))\hat{J}_n(kr')\hat{J}_n(kr)\\
&-\frac{k}{4\pi\omega\mu_0}.\frac{\sin\phi\sin\phi'}{rr'}\sum_{n=1}^{\infty}h_n\frac{2n+1}{n(n+1)}\frac{\partial^2}{\partial\phi\partial\phi'}\\
&\times P_n(\cos(\phi-\phi'))\hat{J}'_n(kr')\hat{J}'_n(kr) \qquad (22)
\end{aligned}
$$

where,

$$
g_n = -\frac{\hat{\boldsymbol{H}}_n^{(2)}(ka)\hat{\boldsymbol{H}}_n^{(2)'}(k0a)-\sqrt{\varepsilon_{ra}}\hat{\boldsymbol{H}}_n^{(2)'}(ka)\hat{\boldsymbol{H}}_n^{(2)'}(k0a)}{\hat{\boldsymbol{J}}_n(ka)\hat{\boldsymbol{H}}_n^{(2)'}(k0a)-\sqrt{\varepsilon_{ra}}\hat{\boldsymbol{J}}'_n(ka)\hat{\boldsymbol{H}}_n^{(2)}(ka)} \qquad (23)
$$

$$
h_n = -\frac{\hat{\boldsymbol{H}}_n^{(2)'}(ka)\hat{\boldsymbol{H}}_n^{(2)}(k0a)-\sqrt{\varepsilon_{ra}}\hat{\boldsymbol{H}}_n^{(2)}(ka)\hat{\boldsymbol{H}}_n^{(2)'}(k0a)}{\hat{\boldsymbol{J}}'_n(ka)\hat{\boldsymbol{H}}_n^{(2)'}(k0a)-\sqrt{\varepsilon_{ra}}\hat{\boldsymbol{J}}'_n(ka)\hat{\boldsymbol{H}}_n^{(2)'}(ka)} \qquad (24)
$$

where the dash represents the derivative of the function. After obtaining the particular and homogeneous parts separately, the magnetic field coupled to DRA is:

$$
H_x^{DRA}(\bar{M}_x^2) = G_{spc} + \iint\limits_{slot} G_{HS}e_p^2\left(x'\right)ds' \qquad (25)
$$

2.2. Evalauation Slot Electric Field

On employing the Galerkin's procedure of testing in Equations (1) and (2) using testing function is same as the basis as given in (5).

$$
\begin{aligned}
&-\left\langle\left[H_x^{WG}\left(M_x^1\right)+H_x^{SL}\left(M_x^1\right)\right],e_q^1(x)\right\rangle\\
&+\left\langle\left[H_x^{SL}\left(M_x^2\right)\right],e_q^1(x)\right\rangle=-2\left\langle H_x^{inc},e_q^1(x)\right\rangle \qquad (26)
\end{aligned}
$$

$$
\begin{aligned}
&\left\langle\left[H_x^{SL}\left(M_x^1\right)\right],e_q^2(x)\right\rangle-\left\langle\left[H_x^{SL}\left(M_x^2\right)\right],e_q^2(x)\right\rangle\\
&+\left\langle\left[H_x^{DRA}\left(M_x^2\right)\right],e_q^2(x)\right\rangle=0 \qquad (27)
\end{aligned}
$$

$$
\Rightarrow\begin{pmatrix}Y_{11} & Y_{12}\\ Y_{21} & Y_{22}\end{pmatrix}\begin{pmatrix}E_{yp}^1\\ E_{yp}^2\end{pmatrix}=\begin{pmatrix}-2H_x^{inc}\\ 0\end{pmatrix} \qquad (28)
$$

On multiplying the weighing function with the corresponding fields as per the Equations (26) and (27), the elements of the moment matrix are:

$$\begin{aligned}\left\langle H_x^{inc}, e_q^1(x)\right\rangle &= -2WL\left[\sin\left\{\frac{\pi x_w}{2a}+\frac{q\pi}{2}\right\}\operatorname{sinc}\left\{\frac{\pi L}{2a}+\frac{q\pi}{2}\right\}\right.\\ &\quad\left.-\sin\left\{\frac{\pi x_w}{2a}-\frac{q\pi}{2}\right\}\operatorname{sinc}\left\{\frac{\pi L}{2a}-\frac{q\pi}{2}\right\}\right] \qquad (29)\end{aligned}$$

$$\begin{aligned}&\left\langle\left[H_x^{WG}\left(M_x^i\right)\right], e_q^i(x)\right\rangle =\\ &-W_i^2L_i^2\sum_{p=1}^{M}E_{yp}^i\sum_m^\infty\sum_n^\infty\frac{ab}{(mb)^2+(na)^2}\left[\frac{m^2}{a}\varepsilon_m\varepsilon_nY_{mn}^e+\frac{4n}{b^2}Y_{mn}^m\right]\\ &\times\cos^2\left\{\frac{n\pi}{2b}(y_w+b)\right\}\operatorname{sinc}^2\left\{\frac{n\pi}{2b}W_i\right\}F_x(p)F_x(q) \qquad (30)\end{aligned}$$

$$\begin{aligned}&\left\langle H_x^{SL}(M_i^x), e_q^i(x)\right\rangle =\\ &-\frac{j\omega\varepsilon}{k^2}\frac{L_sW_sL_oW_o}{a_2b_2}\sum_{p=1}^{M}E_{yp}^i\sum_{m=1}^\infty\sum_{n=0}^\infty\varepsilon_m\varepsilon_n\left\{k^2-\left(\frac{m\pi}{2a_2}\right)^2\right\}\\ &\times\cos\left\{\frac{n\pi}{2b_2}(y_{ws}+b_2)\right\}\operatorname{sinc}\left\{\frac{n\pi}{2b_2}W_s\right\}\cos\left\{\frac{n\pi}{2b_2}(y_{wo}+b_2)\right\}\operatorname{sinc}\left\{\frac{n\pi}{2b_2}W_o\right\}\\ &\times\frac{\{-F_{xs}(p)F_{xo}(q)\}}{\Gamma_{mn}\sin\{2\Gamma_{mn}t\}}\begin{cases}\cos\{\Gamma_{mn}(z-t)\}\cos\{\Gamma_{mn}(z_0+t)\} & z>z_0\\ \cos\{\Gamma_{mn}(z_0-t)\}\cos\{\Gamma_{mn}(z+t)\} & z<z_0\end{cases} \qquad (31)\end{aligned}$$

where 'o' stands for observation or field location and 's' for source location. In the above equations since both the aperture dimensions remains same, therefore, $W_1 = W_2$, $L_1 = L_2$, $L_s = L_0$ and $W_s = W_0$.

The final term, i.e., on testing the field within the DRA is

$$\begin{aligned}&\left\langle\left[H_x^{DRA}\left(M_x^2\right)\right], e_q^2(x)\right\rangle =\\ &\left\langle[G_{spc}], e_q^2(x)\right\rangle+\iint_{slot}\iint_{slot}G_{HS}e_p^2(x')\,e_q^2(x)\,ds'ds \qquad (32)\end{aligned}$$

The second part of integration (32) is directly computed in time domain by quad integral in programme. The first part of (32) after

taking the reaction;

$$\left\langle [G_{spc}], e_q^2(x) \right\rangle = -\frac{4W^2L^2}{\pi^2 k\eta} \int_{-\infty}^{\infty}\int_{-\infty}^{\infty} \frac{k^2 - k_x^2}{\left(k^2 - k_x^2 - k_y^2\right)^{1/2}} \mathrm{sinc}^2(k_y W) \times \frac{\begin{Bmatrix} \sin^2(k_x L) & \text{p, q both even} \\ \cos^2(k_x L) & \text{p, q both odd} \\ 0 & \text{otherwise} \end{Bmatrix}}{\frac{p\pi}{2}\left\{1-\left(\frac{2Lk_x}{p\pi}\right)^2\right\}\frac{q\pi}{2}\left\{1-\left(\frac{2Lk_x}{q\pi}\right)^2\right\}} dk_x dk_y \quad (33)$$

To carry out this integral (33) in the spectral domain, we make the following substitutions to obtain the real and imaginary parts of the integral. The real part is obtained by evaluating the integral given by (33) for $k_x^2 + k_y^2 \le k^2$,and the imaginary part by evaluating the integral for $k_x^2 + k_y^2 \ge k^2$. These two regions correspond to the visible region (radiation field) and the invisible region (evanescent field) respectively.

In the visible region, $k_x^2 + k_y^2 \le k^2$

$$k_x = k\sin\theta\cos\phi \quad (34)$$

$$k_y = k\sin\theta\sin\phi \quad (35)$$

$$dk_x dk_y = k^2\sin\theta\cos\theta d\theta d\phi \quad (36)$$

in the invisible region, $k_x^2 + k_y^2 \le k^2$

$$k_x = k\cosh\theta\cos\phi \quad (37)$$

$$k_y = k\cosh\theta\sin\phi \quad (38)$$

$$dk_x dk_y = k^2\sinh\theta\cosh\theta d\theta d\phi \quad (39)$$

After making the substitution of the above equations, the modified expression of (33) is:

$$\left\langle [G_{spc}], e_p^2(x) \right\rangle\big|_{visible\ region} =$$

$$-\frac{16W^2L^2}{\lambda^2\eta} \int_{\theta=0}^{\pi/2}\int_{\phi=0}^{2\pi} \left(1-\sin^2\theta\cos^2\phi\right)\mathrm{sinc}^2(Wk\sin\theta\sin\phi) \times \frac{\begin{Bmatrix} \sin^2(Lk\sin\theta\cos\phi) & \text{for p, q both even} \\ \cos^2(Lk\sin\theta\cos\phi) & \text{for p, q both odd} \\ 0 & \text{otherwise} \end{Bmatrix}}{\frac{p\pi}{2}\frac{q\pi}{2}\left\{1-\left(\frac{2Lk\sin\theta\cos\phi}{p\pi}\right)\right\}\left\{1-\left(\frac{2Lk\sin\theta\cos\phi}{q\pi}\right)\right\}} \sin\theta d\theta d\phi \quad (40)$$

$$\left\langle [G_{spc}], e_p^2(x) \right\rangle \big|_{invisible\ region} =$$

$$-j\frac{16W^2L^2}{\lambda^2\eta}\int_{\theta=0}^{\infty}\int_{\phi=0}^{2\pi}\left(1-\cosh^2\theta\cos^2\phi\right)\mathrm{sinc}^2\left(Wk\cosh\theta\sin\phi\right)$$

$$\times\frac{\left\{\begin{matrix}\sin^2\left(Lk\cosh\theta\cos\phi\right) & \text{for p, q both even}\\ \cos^2\left(Lk\cosh\theta\cos\phi\right) & \text{for p, q both odd}\\ 0 & \text{otherwise}\end{matrix}\right\}}{\frac{p\pi}{2}\frac{q\pi}{2}\left\{1-\left(\frac{2Lk\cosh\theta\cos\phi}{p\pi}\right)\right\}\left\{1-\left(\frac{2Lk\cosh\theta\cos\phi}{q\pi}\right)\right\}}\cosh\theta d\theta d\phi \tag{41}$$

3. EVALUATION OF REFLECTION COFFICIENT

To determine the reflection coefficient, we decouple the sources, one at $-\infty$ in the feed waveguide and the other at the window. The incident electric field due to the TE_{10} excitation at the $z = 0$ plane is:

$$E_y^{inc} = \cos\left(\frac{\pi x}{2a}\right) \tag{42}$$

When the window aperture is shorted, the electric field is the field reflected by the electric short circuit and is given by,

$$E_y^1 = -\cos\left(\frac{\pi x}{2a}\right) \tag{43}$$

When the generator in the feed waveguide is removed and replaced by a perfect match, the electric field for the dominant TE_{10} mode scattered by the window into the waveguide is by substituting $m = 1$, $n = 0$, at the $z = 0$ plane as:

$$E_y^2 = \sum_{p=1}^{M} E_{yp}^1\frac{WL}{ab}\left[\cos\left\{\frac{\pi}{2}\left(-\frac{x_w}{a}+p-1\right)\right\}\mathrm{sinc}\left\{\frac{\pi L}{2}\left(\frac{p}{L}-\frac{1}{a}\right)\right\}\right.$$
$$\left.-\cos\left\{\frac{\pi}{2}\left(\frac{x_w}{a}+p+1\right)\right\}\mathrm{sinc}\left\{\frac{\pi L}{2}\left(\frac{p}{L}+\frac{1}{a}\right)\right\}\right]\cos\left(\frac{\pi x}{2a}\right) \tag{44}$$

Reflection coefficient Γ can then be expressed as:

$$\Gamma = \frac{E_y^1 + E_y^2}{E_y^{inc}} = -1 + \frac{WL}{ab}\sum_{p=1}^{M} E_{yp}^1 \left[\cos\left\{\frac{\pi}{2}\left(-\frac{x_w}{a} + p - 1\right)\right\}\operatorname{sinc}\left\{\frac{\pi L}{2}\left(\frac{p}{L} - \frac{1}{a}\right)\right\} - \cos\left\{\frac{\pi}{2}\left(\frac{x_w}{a} + p + 1\right)\right\}\operatorname{sinc}\left\{\frac{\pi L}{2}\left(\frac{p}{L} + \frac{1}{a}\right)\right\}\right] \quad (45)$$

Then the coupled power

$$Pc/Pin = 1 - |\Gamma| \quad (46)$$

4. COMPUTED AND MEASURED RESULTS

To implement the theory presented in this work, a general MATLAB code was written capable of analyzing hemispherical DRA excited by a thick slot, kept at the offset in both x and y directions. Convergence checks for the moment method solution were performed. It was found that convergence is very stable, and results using number of basis function, $N = 1$ were very close to those using larger N. Fig. 3 shows

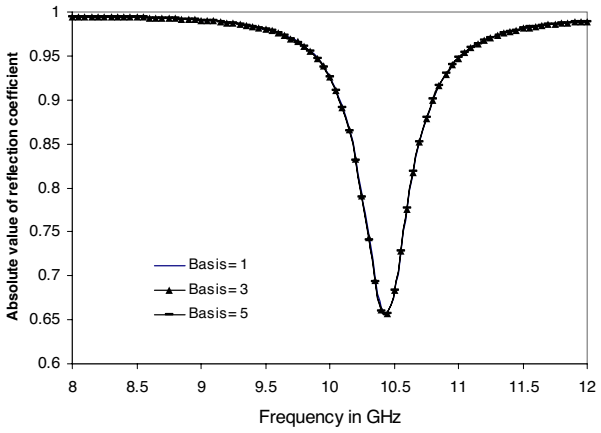

Figure 3. Comparing the reflection coefficient computed for different numbers of basis functions. Slot dimensions of WR90 waveguide are: 9.2 mm × 0.3 mm, thickness of slot 1.3 mm, DRA of $\varepsilon_r = 10$ and radius = 6.27 mm.

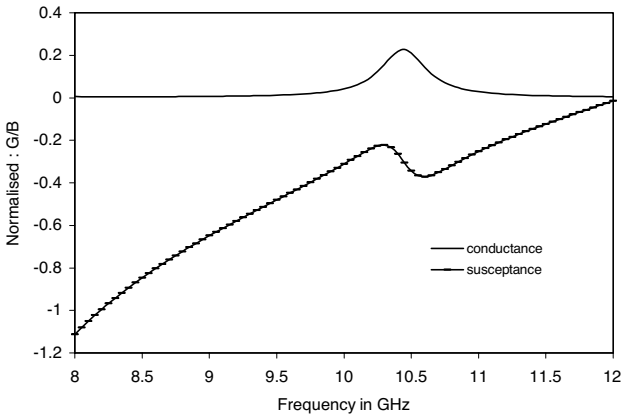

Figure 4. Computed normalized admittance at the slot aperture: dimensions of slot of WR90 waveguide are: 9.2 mm × 0.3 mm, thickness of slot 1.3 mm, DRA of $\varepsilon_r = 10$ and radius = 6.27 mm.

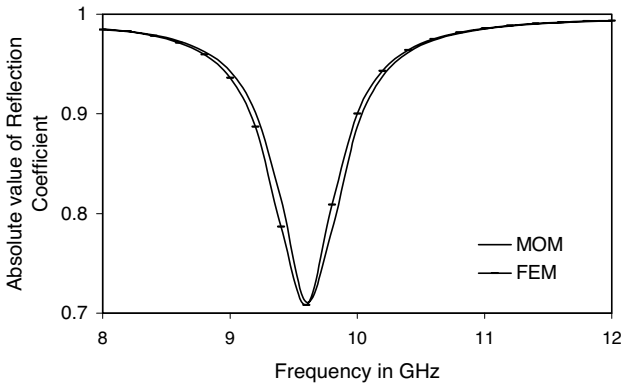

Figure 5. Comparing, computed reflection coefficient with HFSS simulation software: dimensions of slot of WR90 waveguide are: 7 mm × 0.3 mm, thickness of slot = 1.3 mm, radius of DRA = 6 mm; $\varepsilon_r = 10.5$.

the absolute value of reflection coefficient for various number of basis function. It is clear that the variation of the computed value from basis function 1 to 5 is negligibly small. In this paper $N = 5$ is used for all calculations. Fig. 4 shows the plot of the computed normalized conductance and susceptance for a slot dimension of 9.2 mm × 0.3 mm size with slot thickness 1.3 mm. In all computations the ground plane is assumed infinity in x and y direction. Fig. 5 comparing

the computed reflection coefficient with the commercial FEM code (Ansoft HFSS) [22] for the slot dimensions of 7 mm × 0.3 mm of 1.3 mm thickness. The radius and permittivity of the hemispherical DRA considered was 6 mm and 10.5 respectively.

To validate the code, an experiment was conducted, with a finite ground plane of 1.27 mm thickness, and square size of 120 mm × 120 mm in which slot is milled with dimension 9.2 mm × 1.0 mm. A hemispherical DRA of radius $a = 6.27$ mm, $\varepsilon_r = 10$ and standard WR90 waveguide with dimensions 22.86 mm × 10.16 mm was used in the measurements. Since the fundamental mode of the 6.27 mm radius DRA is 7.15 GHz, it is excited at TE_{221} mode in the X-band. Fig. 6 comparing the computed and measured results of power coupled with the FEM code. The discrepancy between theory and experiment is mainly due to the non uniform air gap between the DRA and ground plane. It has been found in simulation that, for a 0.05 mm thick uniform air gap introduced between the slot and DRA, the resonant frequency is shifting from 9.9 GHz to 11.1 GHz and the coupled power is increasing from 0.3 to 0.39. After the fabrication, it is observed that the ground plane surface was not perfectly flat, it introduced non uniform air gap. Furthermore, the fabrication tolerances of slot have also gives rise to mismatch between theory and experiment.

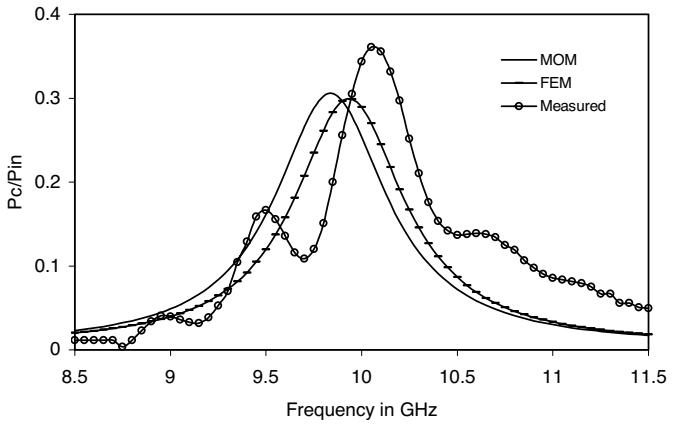

Figure 6. Comparing the measured coupled power through the slot with MOM and HFSS Slot dimensions: 9.2 mm × 1.0 mm, thickness of slot 1.3 mm, DRA of $\varepsilon_r = 10$ and radius = 6.27 mm.

5. PARAMETRIC STUDIES

There are many design parameters involved in the problem under consideration. Since the effective permittivity seen by the slot is not exactly known, the resonant length is not well defined. The slot is made on a thick ground plane, the thickness and width of slot will influence the resonant frequency and depth of return loss. Further parameters include DRA radious and permittivity. The design parameters can be optimized to achieve maximum coupling, large bandwidth, dual band operation, a specific radiation pattern or a combination of those according to the design requirements. This section gives the observed simulation results when the parameters discussed above are systematically varied. The simulations are carried out using the developed code. In all the results presented below, the WR90 waveguide with dimensions 22.86 mm × 10.16 mm is used for the excitation. A hemispherical DRA of radius $a = 6.27$ mm, $\varepsilon_r = 10$ is considered centered to the waveguide end and ground plane. In the results follow, a sensitivity analysis of the power coupled versus frequency is provided.

5.1. Varying Slot Dimensions

Viewing the thick ground plane as a secondary waveguide having relatively small cross sectional dimensions (the dimensions of the slot) explains readily the effect of wall thickness. Since small waveguide dimension means high cut off frequency, the coupled power through the slot to DRA should have been decreased as the thickness increased. Fig. 7 shows the variation of power coupled as the thickness of slot is varied from 0 to 1.2 mm while keeping the length and width of slot same. It is found that the matching to the DRA is improving with shifts in frequency as the thickness is increased. This is because of the loading effect of DRA to the slot.

In Fig. 8, the variation of power coupled is shown as the slot length, $2L$, is varied from 8.0 to 8.4 mm while the width, $2W$, is maintained 0.5 mm. All other parameters such as position of slot and thickness of slot remain same. It is observed that, the resonance shifts up with decreasing slot length. Similar results are shown in Fig. 9, when the slot width, $2W$ is varied from 0.3 to 0.5 mm while the length is maintained 9 mm. These results provide evidence that both slot length and slot width can be used for tuning the desired resonance frequency.

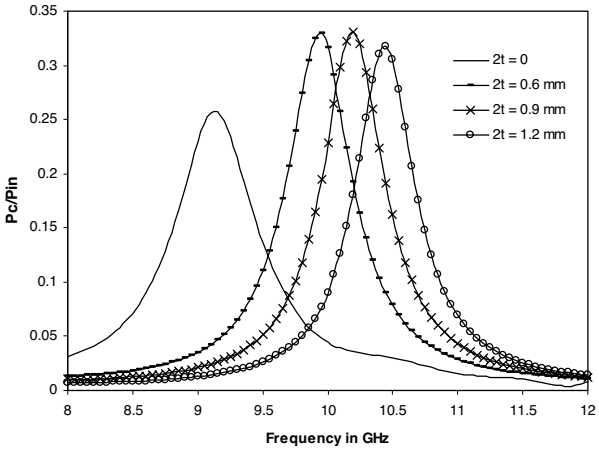

Figure 7. The effects of the slot thickness on the coupled power through the slot with slot dimensions: 8.4 mm × 0.6 mm and DRA of $\varepsilon_r = 10$ and radius 6.27 mm.

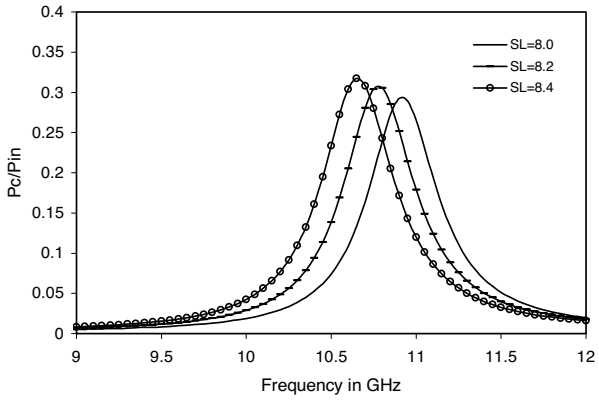

Figure 8. The effects of the slot length on the coupled power through the slot with slot dimensions: 0.5 mm wide and 1.3 mm thick. DRA of $\varepsilon_r = 10$ and radius 6.27 mm.

5.2. Varying Slot Position

The resonant frequency and power coupled both can be controlled by giving offset to the slot along x and y-directions. While keeping DRA at the center of the ground plane and moving the slot from center will excite the DRA in its higher order modes. In Fig. 10, the variation of power coupled and resonant frequency as the slot moved from center

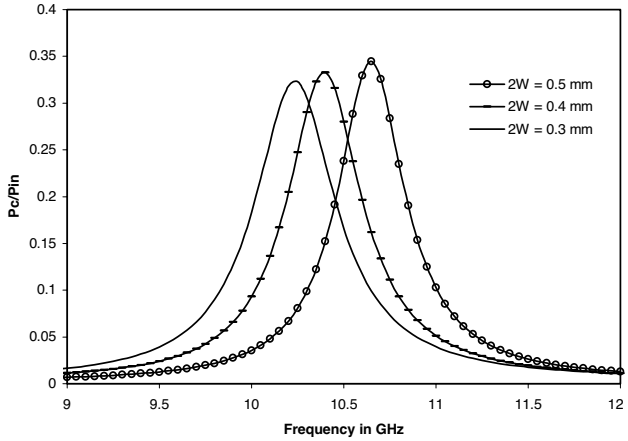

Figure 9. The effects of the slot width on the coupled power through the slot with slot dimensions: 9.0 mm long and 1.3 mm thick. DRA of $\varepsilon_r = 10$ and radius 6.27 mm.

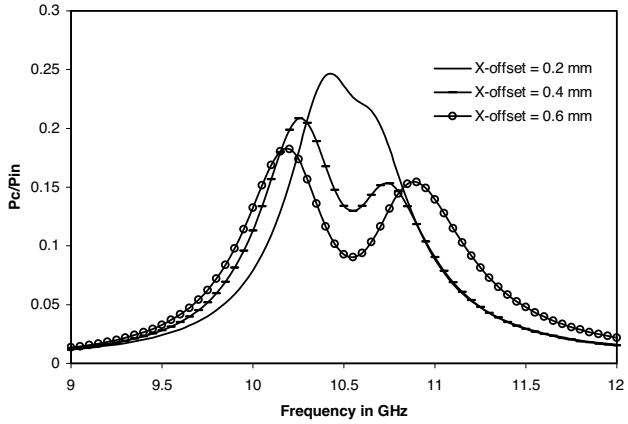

Figure 10. The effects of the slot position along x-direction on the coupled power through the slot with slot dimensions: 8.2 mm $\times$ 0.8 mm, 1.3 mm thick. DRA of $\varepsilon_r = 10$ and radius 6.27.

to one end along x-direction, while keeping the DRA at the center of the ground plane. It is observed that, while increasing the offset it starts giving second resonance at lower frequency band and when the offset is more than 0.6 mm it gives dual resonance characteristics. Almost similar characteristic is showing when the slot is moved along y-direction. Fig. 11 shows the effect of moving the slot along y axis by

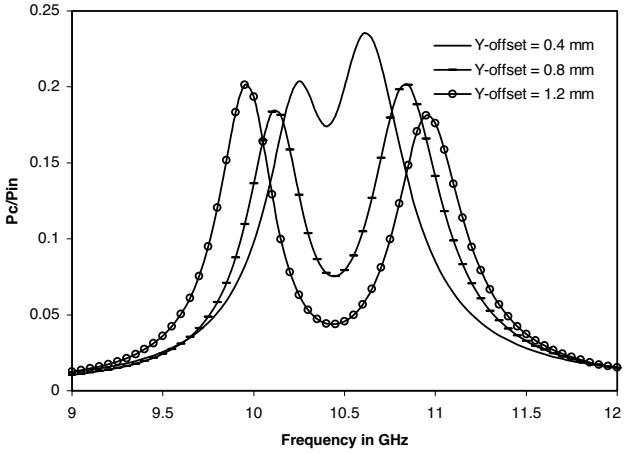

Figure 11. The effects of the slot position along y-direction on the coupled power through the slot with slot dimensions: 8.2 mm × 0.8 mm, 1.3 mm thick. DRA of $\varepsilon_r = 10$ and radius 6.27.

keeping the DRA at the center. By giving small offset either in x or y direction, it is found that the bandwidth can be increased. This is because both DRA resonance and slot resonance are merging together.

REFERENCES

1. Long, S. A., M. W. McAllister, and L. C. Shen, "The resonant cylindrical dielectric resonator antenna," *IEEE Trans. Antennas Propagt.*, Vol. 31, 406–412, May 1983.
2. Betzios, P. V., I. S. Karanasiou, and N. K. Uzunoglu, "Analysis of a dielectric resonator antenna by applying a combined semi-analytical method and simulation," *J. of Electromagn. Waves and Appl.*, Vol. 21, No. 14, 1983–1994, 2007.
3. Song, Y. and A. R. Sebak, "Radiation pattern of aperture coupled prolate hemispheroidal dielectric resonator antenna," *Progress In Electromagnetics Research*, PIER 58, 115–133, 2006.
4. Tadjalii, A., A. Sebak, and T. A. Denidni, "Resonance frequencies and far field patterns of elliptical dielectric resonator antenna: Analytical approach," *Progress In Electromagnetics Research*, PIER 64, 81–98, 2006.
5. Kishk, A. A., M. R. Zonoubi, and D. Kajfez, "A numerical study of a dielectric disc antenna above grounded dielectric substrate,"

IEEE Trans. on Antenna Propagation, Vol. 41, No. 6, 813–821, 1993.

6. Kumar, A. V. P., V. Hamsakutty, J. Yohannan, and K. T. Mathew, "Microstripline FED cylindrical dielectric resonator antenna with a coplanar parasitic strip," *Progress In Electromagnetics Research*, PIER 60, 143–152, 2006.
7. Kishk, A. and A. W. Glisson, "Bandwidth enhancement for split cylindrical dielectric resonator antenna," *Progress In Electromagnetics Research*, PIER 33, 97–118, 2001.
8. Rezaei, P., M. Hakkak, and K. Forooraghi, "Design of wideband dielectric resonator antenna with a two segment structure," *Progress In Electromagnetics Research*, PIER 66, 111–124, 2006.
9. Leung, K. W., K. M. Luk, K. Y. A. Lai, and D. Lin, "Theory and experiment of a coaxial probe-fed hemispherical dielectric resonator antenna," *IEEE Trans. Antennas Propagat.*, Vol. 41, 1390–1398, Oct. 1993.
10. Petosa, A., R. K. Mongia, A. Ittipiboon, and J. S. Wight, "Design of microstrip fed series array of dielectric resonator antennas," *Electron. Lett.*, Vol. 31, No. 16, 1306–1307, Aug. 1995.
11. Saed, M. and R. Yadla, "Microstrip-fed low profile and compact dielectric resonator antennas," *Progress In Electromagnetics Research*, PIER 56, 151–162, 2006.
12. Leung, K. W., K. Y. A. Lai, K. M. Luk, and D. Lin, "Input impedance of aperture coupled hemispherical dielectric resonator antenna," *Electron. Lett.*, Vol. 29, 1165–1167, June 1993.
13. Kranenburg, R. A., S. A. Long, and J. T.Williams, "Coplanar waveguide excitation of dielectric resonator antennas," *IEE Trans. Antennas Propagat.*, Vol. 39, 119–122, Jan. 1991.
14. Rao, Q., T. A. Denidni, A. R. Sebak, and R. H. Johnston, "On improving impedance matching of a CPW fed low permittivity dielectric resonator antenna," *Progress In Electromagnetics Research*, PIER 53, 21–29, 2005.
15. Leung, K. W., "Conformal strip excitation of dielectric resonator antenna," *IEEE Antennas and Propagation Society International Symposium Digest*, Vol. 2, 132–135, Boston Massachusettes, USA, July 2001.
16. Eshrah, I. A., A. A. Kishk, A. B. Yakovlev, and A. W. Glisson. "Theory and implementation of dielectric resonator antenna excited by a waveguide slot," *IEEE Antennas and Propagat.*, Vol. 53, No. 1, 483–494, January 2005.
17. Lueng, K. W., K. W. Luk, K. Y. A. Lai, and D. Lin, "Theory

and experiment of an aperture-coupled hemispherical dielectric resonator antenna," *IEEE Trans. Antennas Propagat.*, Vol. 43, No. 11, 1192–1198, November 1995.

18. Paramesha, S. and A. Chakrabarty, "Moment method ananlysis of rectangular waveguide as near field measuring probe," *Microwave and Opti. Technol. Lett.*, Vol. 48, 1802–1805, 2006.
19. Mandal, M. and A. Chakraborty, " Resonant length calculation and radiation pattern synthesis of longitudinal slot antenna in rectangular waveguide," *Progress In Electromagnetics Research Letters*, Vol. 3, 187–195, 2008.
20. Das, S. and A. Chakrabarty, " A novel modeling technique to solve a class of rectangular waveguide based circuits and radiators," *Progress In Electromagnetics Research*, PIER 61, 231–252, 2006.
21. Das, S., A. Chakrabarty, and A. Chakraborty, "Characteristics of an offset longitudinal/transverse slot coupled crossed waveguide junction using multiple cavity modelling technique considering the mode at the slot aperture," *Progress In Electromagnetics Research*, PIER 67, 297–316, 2007.
22. Ansoft High Frequency Structures Simulator (HFSS), version 11.0, Ansoft Corporate. USA.
23. Harrington, R. F., *Time Harmonic Electromagnetic Fields*, 389–391, McGraw-Hill Book Company, New York, USA, 1961.